Contribution from the Dipartimento di Chimica Inorganica e Metallorganica and Istituto di Chimica Strutturistica Inorganica, Università degli Studi di Milano, Via G. Venezian 21, 20133 Milano, Italy, and Dipartimento di Chimica dell'Università, Pian dei Mantellini 44, 53100 Siena, Italy

Iron–Iridium Mixed-Metal Carbonyl Clusters. 3.[2] Synthesis, Chemical Characterization, Electrochemical Behavior, and Solid-State Structures of $[NEt_4]_3[FeIr_5(CO)_{15}]$, $[NMe_3(CH_2Ph)]_2[HFeIr_5(CO)_{15}]$, and $[NMe_3(CH_2Ph)][FeIr_5(CO)_{16}]$. Spectroscopic and Chemical Evidence for the Existence of $[HFe_3Ir(CO)_{12}]^{2-}$, $[H_2Fe_3Ir(CO)_{12}]^-$, and $[H_2FeIr_5(CO)_{15}]^-$

Alessandro Ceriotti,[1a] Roberto Della Pergola,*[,1a] Luigi Garlaschelli,[1a] Franco Laschi,[1c] Mario Manassero,[1b] Norberto Masciocchi,*[,1b] Mirella Sansoni,[1b] and Piero Zanello*[,1c]

Received January 11, 1991

The reaction of $[HFe(CO)_4]^-$ with $Ir(CO)_3Br$ (in molar ratio 3:1) produced $[HFe_3Ir(CO)_{12}]^{2-}$ (**1**), which reacts with acids to yield the dihydride complex $[H_2Fe_3Ir(CO)_{12}]^-$ (**2**). The salt $[NEt_4]_2[HFe_3Ir(CO)_{12}]$ crystallizes in the orthorhombic space group *Pnma*, with $a = 20.346$ (7) Å, $b = 15.135$ (2) Å, $c = 11.807$ (5) Å, $V = 3636$ (1) Å^3, and $Z = 4$; a full structural determination was prevented by the poor quality of the crystals. The reaction of $[FeIr_4(CO)_{15}]^{2-}$ with $[Ir(CO)_4]^-$, in refluxing acetonitrile, has yielded the new compound $[FeIr_5(CO)_{15}]^{3-}$ (**3**). The trianion reacts with stoichiometric amount of H^+ to form $[HFeIr_5(CO)_{15}]^{2-}$ (**4**) and with acids in excess to yield the corresponding dihydride derivative $[H_2FeIr_5(CO)_{15}]^-$ (**5**), which, at room temperature, is not stable and is readily transformed into $[FeIr_5(CO)_{16}]^-$ (**6**). The salts of **3**, **4**, and **6** were characterized by single-crystal X-ray analyses. $[NEt_4]_3[FeIr_5(CO)_{15}]$ crystallizes in the triclinic space group $P\bar{1}$, with $a = 18.827$ (5) Å, $b = 19.476$ (6) Å, $c = 18.064$ (5) Å, $\alpha = 117.06$ (3)°, $\beta = 90.76$ (2)°, $\gamma = 61.71$ (2)°, and $Z = 4$. The octahedral carbonyl cluster contains 12 terminal and three edge-bridging carbonyl groups. $[NMe_3(CH_2Ph)]_2[HFeIr_5(CO)_{15}]$ crystallizes in the triclinic space group $P\bar{1}$, with $a = 10.218$ (3) Å, $b = 10.989$ (4) Å, $c = 20.757$ (5) Å, $\alpha = 101.07$ (2)°, $\beta = 97.61$ (2)°, $\gamma = 108.13$ (2)°, and $Z = 2$. The octahedral metal framework of the hydrido carbonyl cluster is surrounded by 11 terminal and four edge-bridging carbonyl groups; the hydrogen atom was located from the X-ray data and it is terminally bonded to iridium with a Ir–H distance of 1.60 (9) Å. $[NMe_3(CH_2Ph)][FeIr_5(CO)_{16}]$ crystallizes in the triclinic space group $P\bar{1}$, with $a = 9.727$ (2) Å, $b = 16.296$ (2) Å, $c = 22.056$ (2) Å, $\alpha = 79.99$ (2)°, $\beta = 80.61$ (2)°, $\gamma = 83.83$ (1)°, and $Z = 4$. The metal carbonyl cluster possess a metal cage based on an octahedral unit surrounded by 12 terminal and four face bridging carbonyl groups. The electrochemical study of the redox propensity of $[FeIr_5(CO)_{16}]^-$ and $[FeIr_5(CO)_{15}]^{3-}$ allowed us to elucidate the mechanistic aspects of their interconversion.

Introduction

Recently, we reported the preparation and the chemical behavior of several tetra- and pentanuclear Fe–Ir mixed-metal carbonyl clusters.[2,3] During these studies, we had only little evidence for the existence of bimetallic clusters containing the "Fe_3Ir" metal core, the missing element in our series of tetrahedral mixed-metal carbonyl clusters, and no evidence of hexanuclear metal carbonyl derivatives. The tetra- and pentanuclear carbonyl clusters have been prepared by employing several iridium and iron carbonyl complexes, as precursors, and the syntheses of the different mixed-metal Fe–Ir carbonyl clusters has been achieved either by redox condensation or by reductive carbonylation.[2,3]

In order to extend the chemistry of the tetranuclear Fe–Ir carbonyl clusters, we have now studied the reactivity of some other iridium complexes toward iron carbonyl derivatives, and in this context, we report here the synthesis and the chemical characterization of two stable hydridic compounds, $[HFe_3Ir(CO)_{12}]^{2-}$ (**1**) and $[H_2Fe_3Ir(CO)_{12}]^-$ (**2**).

Starting from $[FeIr_4(CO)_{15}]^{2-}$ and $[Ir(CO)_4]^-$, the first hexanuclear Fe–Ir carbonyl cluster $[FeIr_5(CO)_{15}]^{3-}$ (**3**) was isolated; the reaction of this compound with acids produced the related hydrido derivatives $[HFeIr_5(CO)_{15}]^{2-}$ (**4**) and $[H_2FeIr_5(CO)_{15}]^-$ (**5**). The latter species is unstable at room temperature and is transformed into $[FeIr_5(CO)_{16}]^-$ (**6**).

All these derivatives have been fully characterized by combination of IR spectroscopy, fast atom bombardment mass spectroscopy, and ^1H NMR spectra. The results of these studies are reported here together with the solid-state structures for the salts of complexes **3**, **4**, and **6**, as determined by single-crystal X-ray diffraction analysis. Finally, the electrochemistry of derivatives **3** and **6** is presented.

Results

Preparation of $[HFe_3Ir(CO)_{12}]^{2-}$ (1) and $[H_2Fe_3Ir(CO)_{12}]^-$ (2). It is known that the reaction of a large excess of $[HFe(CO)_4]^-$ with $[Ir(CO)_2Cl_2]^-$ proceeds slowly at room temperature with the formation, in high yield, of $[Fe_2Ir_2(CO)_{12}]^{2-}$.[2] On the contrary, the same reaction performed in refluxing tetrahydrofuran (thf) produced a mixture of $[HFe_3Ir(CO)_{12}]^{2-}$ (**1**) and $[Fe_2Ir_2(CO)_{12}]^{2-}$, where the new hydridic compound **1** is the major component present in the solution. The same type of mixture is also obtained when the polymeric $Ir(CO)_3Br$ is used as source of Ir(I). The reaction of $[HFe_3(CO)_{11}]^-$ and $[Ir(CO)_4]^-$, in the molar ratio 1:1, was also tested in order to obtain a more selective synthesis of **1**, since Fe, Ir, and the negative charges are present in the correct ratio. Instead, the reaction proceeds with a different stoichiometry, in refluxing acetone, with the selective formation of $[Fe_2Ir_2(CO)_{12}]^{2-}$, apparently according to the following equation:

$$[HFe_3(CO)_{11}]^- + 2[Ir(CO)_4]^- \rightarrow [Fe_2Ir_2(CO)_{12}]^{2-} + [HFe(CO)_4]^- + 3CO$$

The IR spectrum of selected crystals of the NEt_4 salt of **1**, in CH_3CN solution, shows bands at 1977 m, 1954 sh, 1945 s, 1892 w, 1760 sh, and 1743 mw cm^{-1}. The hydridic nature of the compound was confirmed by ^1H NMR spectrum (in acetone-d_6 solution), which shows, at low temperature (−90 °C), a sharp signal at δ −16.9, shifted to δ −17.5 at room temperature. The crystals of $[NEt_4]_2[HFe_3Ir(CO)_{12}]$[4] are isomorphous with the

(1) (a) Dipartimento di Chimica Inorganica e Metallorganica, Università degli Studi di Milano. (b) Istituto di Chimica Strutturistica Inorganica, Università degli Studi di Milano. (c) Dipartimento di Chimica dell'Università.

(2) Part 2: Della Pergola, R.; Garlaschelli, L.; Demartin, F.; Manassero, M.; Masciocchi, N.; Sansoni, M. *J. Chem. Soc., Dalton Trans.* **1990**, 127.

(3) Della Pergola, R.; Garlaschelli, L.; Demartin, F.; Manassero, M.; Masciocchi, N.; Sansoni, M.; Fumagalli, A. *J. Chem. Soc., Dalton Trans.* **1989**, 1109.

(4) Crystal data for $[NEt_4]_2[HFe_3Ir(CO)_{12}]$: $C_{28}H_{41}Fe_3IrN_2O_{12}$, fw = 956.72, orthorhombic space group *Pnma*, $a = 20.346$ (7) Å, $b = 15.135$ (2) Å, $c = 11.807$ (5) Å, $V = 3636$ Å^3, $Z = 4$, current $R = 0.16$ for 984 reflections with $I > 3\sigma(I)$. The solid-state structure shows a high substitutional disorder in the metal sites and poorly defined carbonyl ligands and cations, which prevented a full structural determination.

0020-1669/91/1330-3349$02.50/0

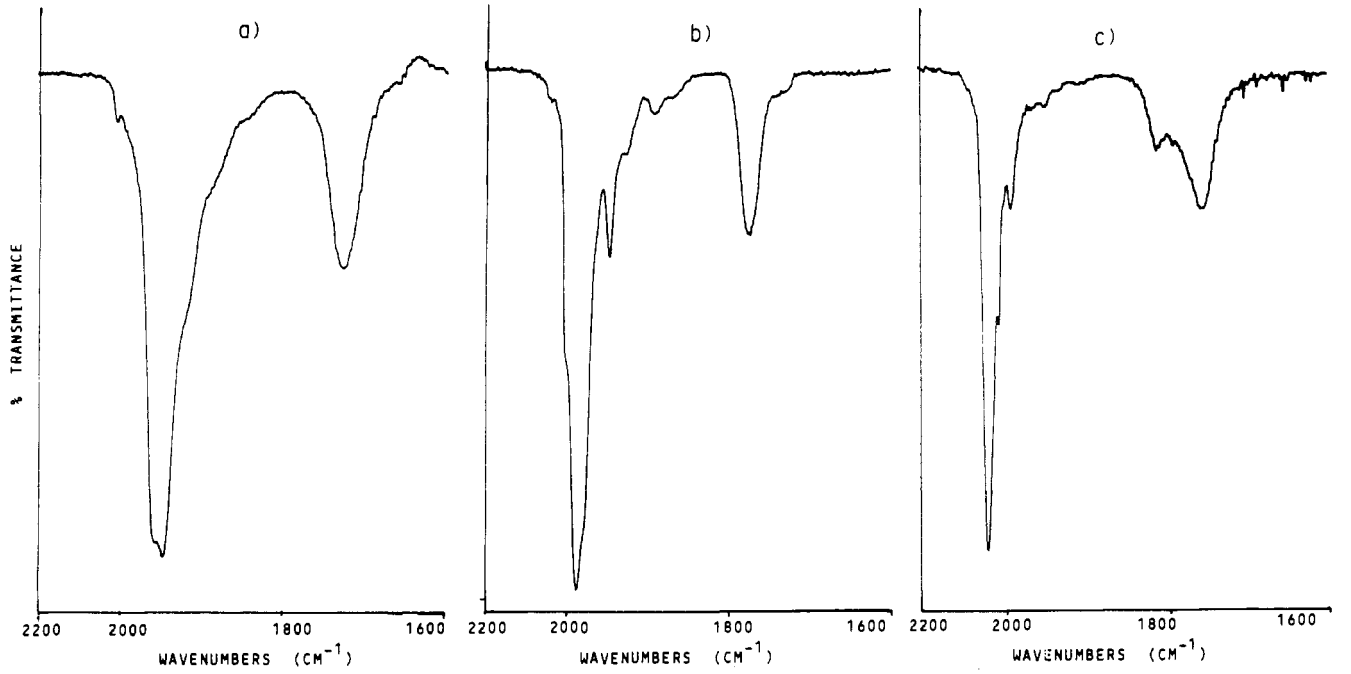

Figure 1. (a) Infrared spectrum of $[NEt_4]_3[FeIr_5(CO)_{15}]$ in CH_3CN. (b) Infrared spectrum of $[N(PPh_3)_2]_2[HFeIr_5(CO)_{15}]$ in THF. (c) Infrared spectrum of $[N(PPh_3)_2][FeIr_5(CO)_{16}]$ in THF.

already structurally characterized $[NEt_4]_2[HFe_3Rh(CO)_{12}]$ and,[5] likely, adopt the same structure in the solid state, that is, the hydride ligand in a face-bridging position (μ_3-H) on the basal Fe_2Ir triangle. However, owing to the poor quality of the crystals, only very poor resolution could be obtained from the X-ray data of **1**, after refinement of the structure. This probably occurred because of cocrystallization of **1** with $[Fe_2Ir_2(CO)_{12}]^{2-}$, which possess a similar metal core but a significantly different ligand shell from **1**, leading to poor molecular packing within the same lattice. The co-crystallization can reasonably explain the presence of small amount of $[Fe_2Ir_2(CO)_{12}]^{2-}$ in all of the samples of **1**, which also causes, sometimes, unsatisfactory elemental analysis.

The addition of small amounts of H_3PO_4 to an acetone solution of **1** causes a shift of the IR bands to higher wavenumbers at 2020 s, 1990 vs, 1980 sh, 1940 m, 1835 m, 1815 m, and 1790 m cm^{-1}, attributable to the dihydridic derivative $[H_2Fe_3Ir(CO)_{12}]^-$ (**2**), which can be crystallized by layering cyclohexane over a thf solution of the NEt_4 salt of **2**. The ^1H NMR spectrum of **2** (in thf-d_8 solution) shows two equally intense signals at δ −23.66 and δ −26.47 at −90 °C; these two signals are due to the two inequivalent hydrogen ligands present in compound **2**. Instead, a unique sharp signal at δ −23.31 can be detected at room temperature; this chemical shift is different from the calculated mean value (δ −25.06) and suggests the presence of different isomers at this temperature. Repeated ^1H NMR experiments, with solutions obtained by dissolving crystalline samples of salts of **2**, invariably shows, at low temperature, signals other than those due to compound **2**; namely, two weaker resonances at δ −19.82 and δ −21.89, which must be assigned to $[HFe_2Ir_2(CO)_{12}]^-$.[2]

Preparation of $[FeIr_5(CO)_{15}]^{3-}$ (3), $[HFeIr_5(CO)_{15}]^{2-}$ (4), $[H_2FeIr_5(CO)_{15}]^-$ (5), and $[FeIr_5(CO)_{16}]^-$ (6). The dianion $[FeIr_4(CO)_{15}]^{2-}$ was found to be a fairly unstable compound,[3] and therefore it was recognized as an useful starting material for the preparation of new clusters.

The reaction of $[FeIr_4(CO)_{15}]^{2-}$ with $[Ir(CO)_4]^-$ in refluxing of CH_3CN produces selectively, within 4 h, the new cluster $[FeIr_5(CO)_{15}]^{3-}$ (**3**), the major impurities being the corresponding monohydride derivative $[HFeIr_5(CO)_{15}]^{2-}$ (**4**) and $[Ir_6(CO)_{15}]^{2-}$. Since $[FeIr_4(CO)_{15}]^{2-}$ and $[Ir(CO)_4]^-$ are available only as salts of very bulky cations, such as $[PPh_4]^+$ or $[N(PPh_3)_2]^+$,[6] compound **3** was also obtained with the same counterions, and the isolation of different salts required a tedious series of metathesis reactions (see Experimental Section). Regardless of the counterions, the salts of **3** are very insoluble in thf as well as in acetone and are very soluble only in CH_3CN. The IR spectrum of the NEt_4 salt of compound **3**, in CH_3CN solution, shows bands at 2004 w, 1942 vs, and 1723 m cm^{-1} (Figure 1a). The addition of carbon monoxide (1 atm, room temperature) to cluster **3** regenerates the two starting materials: $[FeIr_4(CO)_{15}]^{2-}$ and $[Ir(CO)_4]^-$.

Cluster **3** reacts in acetone suspension or in acetonitrile solution with H_3PO_4 to yield, immediately, the hydridic species $[HFeIr_5(CO)_{15}]^{2-}$ (**4**); this cluster is much more soluble than **3**, both in thf and acetone. The IR spectrum of the $[N(PPh_3)_2]^+$ salts of **4**, in thf solution, shows bands at 1987 vs 1946 w, and 1770 s cm^{-1} (Figure 1b); the infrared spectrum of the $[NMe_3(CH_2Ph)]^+$ salt is identical in the terminal carbon monoxide stretching region but shows two broad and weak bands at 1810 and 1790 cm^{-1} probably because of ion pairing effects.[7] The ^1H NMR spectrum (in thf-d_8 solution) shows a clear signal at δ −11.7, with the correct intensity ratio to the cation phenyl hydrogens. Under more strongly protonating conditions (e.g. H_2SO_4 in thf solution), **4** easily adds H^+ to yield $[H_2FeIr_5(CO)_{15}]^-$ (**5**), which shows IR bands at 2040 vs and 1820 m cm^{-1}. The dihydride derivative survives in solution only for a few hours and further reacts, yielding almost exclusively $[FeIr_5(CO)_{16}]^-$ (**6**), with a small amount of insoluble material, deriving from partial decomposition of the starting cluster. We are currently trying to grow crystals of **5** at low temperature. The dihydridic nature of $[H_2FeIr_5(CO)_{15}]^-$ was ascertained by ^1H NMR spectroscopy; the dihydride complex was prepared in the NMR tube, by addition of CF_3CO_2H to a solution of $[HFeIr_5(CO)_{15}]^{2-}$ in deuterated thf and immediately cooled down at low temperature. The ^1H NMR spectrum shows, at −90 °C, two broad signals, at δ −4.5 and δ −14.8 (average value δ −9.65). The two signals disappear at −30 °C, and at −10 °C only one single broad signal appears at δ −9.46, in good agreement with the calculated average value; the signal sharpens readily upon increasing the temperature and becomes very narrow at 25 °C. These data suggest that the hydrogen ligands are located in two very different metallic sites at low temperature and are rapidly exchanging near at room temperature. The salts of

(5) Della Pergola, R.; Garlaschelli, L.; Demartin, F.; Manassero, M.; Masciocchi, N.; Longoni, G. *J. Organomet. Chem.* **1988**, *352*, C59.

(6) Garlaschelli, L.; Chini, P.; and Martinengo, S. *Gazz. Chim. Ital.* **1982**, *112*, 285.

(7) Demartin, F.; Manassero, M.; Sansoni, M.; Garlaschelli, L.; Martinengo, S.; Canziani, F. *J. Chem. Soc., Chem. Commun.* **1980**, 903.

Table I. Selected Distances (Å) and Angles (deg) in the Trianion $[FeIr_5(CO)_{15}]^{3-}$ (**3**) with Estimated Standard Deviations (Esd's) on the Last Figure in Parentheses

Ir(1)–Ir(2)	2.786 (2)	Ir(7)–Ir(8)	2.764 (2)
Ir(1)–Ir(3)	2.841 (1)	Ir(7)–Ir(9)	2.827 (2)
Ir(1)–Ir(4)	2.690 (2)	Ir(7)–Ir(10)	2.736 (2)
Ir(1)–Ir(5)	2.874 (1)	Ir(7)–Ir(11)	2.784 (2)
Ir(2)–Ir(3)	2.789 (2)	Ir(8)–Ir(10)	2.766 (2)
Ir(2)–Ir(4)	2.749 (2)	Ir(8)–Ir(11)	2.775 (2)
Ir(2)–M(6)	2.713 (6)	Ir(8)–M(12)	2.694 (5)
Ir(3)–Ir(5)	2.712 (2)	Ir(9)–Ir(10)	2.780 (2)
Ir(3)–M(6)	2.736 (6)	Ir(9)–Ir(11)	2.728 (2)
Ir(4)–Ir(5)	2.852 (2)	Ir(9)–M(12)	2.765 (4)
Ir(4)–M(6)	2.757 (5)	Ir(10)–M(12)	2.804 (4)
Ir(5)–M(6)	2.730 (6)	Ir(11)–M(12)	2.768 (5)
	Average Values[a]		
M–M	2.767	$M–C_t$	1.799 (30)[b]
$C–O_t$	1.178 (30)[b]	$M–C_b$	1.989 (25)[b]
$C–O_b$	1.209 (27)[b]		
$M–C_t–O_t$	174.6 (2.4)[b]	$M–C_b–O_b$	137.0 (2.1)[b]

[a] Key: M = metal; t = terminal; b = bridging. [b] The numbers in parentheses for the average values are the typical esd's of the single values before averaging.

$[FeIr_5(CO)_{16}]^-$ (**6**) with different bulky cations are very soluble in thf, acetone, and CH_2Cl_2, from which the $N(PPh_3)_2$ salt was crystallized by addition of cyclohexane. The IR spectrum of this compound is very similar to that of **5**, showing bands at 2037 vs, 2008 sh, 1990 w, 1813 m, and 1758 ms cm^{-1} (Figure 1c); the spectra of **5** and **6** differ significantly only in the bridging carbonyl stretching region, since **6** shows bands at lower wavenumbers, attributable to face-bridging ligands as found in the solid-state structure.

Fast Atom Bombardment Mass Spectroscopy. In order to attain a complete characterization of the isolated compounds we also carried out fast atom bombardment mass spectroscopy (FAB-MS) experiments monitoring the negative ions region.

The best results were obtained with compound $[N(PPh_3)_2][FeIr_5(CO)_{16}]$ ($[N(PPh_3)_2][\mathbf{6}]$), probably because of its small negative charge and its intrinsic stability. A very intense signal centered at m/z = 1464 (^{56}Fe, ^{192}Ir) was observed, corresponding to the molecular ion, with an isotopic pattern distribution coincident with the simulated one. Fragmentation with peaks due to the successive loss of 10 carbon monoxide groups are observed down to the limit of m/z = 1184. By contrast, $[NEt_4]_3[FeIr_5(CO)_{15}]$ ($[NEt_4]_3[\mathbf{3}]$), produced signals of low intensity; still, the parent peak at m/z = 1436 (^{56}Fe, ^{192}Ir) and a signal at m/z = 1566, corresponding to the ion pairing of **3** with one $[NEt_4]^+$ cation, were detected. In the same spectral region, however, other small signals, of low intensity, are present, and are probably due either to reorganization of the cluster or to reaction with the matrix. The most reliable peak was found at m/z = 1324 together with the signals due to CO loss and can be reasonably assigned to $[Ir_5(CO)_{13}]^-$, which corresponds to a stable configuration of a still unknown pentanuclear iridium cluster containing 72 cluster valence electrons. For the tetranuclear cluster $[NEt_4]_2[HFe_3Ir(CO)_{12}]$ the parent peak at m/z = 697 (^{56}Fe, ^{192}Ir) was clearly detected along with small traces of the peaks corresponding to $[Fe_2Ir_2(CO)_{12}]^{2-}$. An intense peak at mass 725 can be assigned to M + CO, for the anion $[Fe_3Ir(CO)_{13}]^-$, which was previously obtained in solution by a different method.[2]

Crystal Structures of $[NEt_4]_3[FeIr_5(CO)_{15}]$ ($[NEt_4]_3[\mathbf{3}]$), $[NMe_3(CH_2Ph)]_2[HFeIr_5(CO)_{15}]$ ($[NMe_3(CH_2Ph)]_2[\mathbf{4}]$), and $[NMe_3(CH_2Ph)][FeIr_5(CO)_{16}]$ ($[NMe_3(CH_2Ph)][\mathbf{6}]$). The crystal structures of the three compounds are based on packing of discrete anions and cations; compounds $[NEt_4]_3[\mathbf{3}]$, and $[NMe_3(CH_2Ph)][\mathbf{6}]$ possess two independent moieties per asymmetric unit. Selected bond distances and angles for the compounds $[NEt_4]_3[\mathbf{3}]$, $[NMe_3(CH_2Ph)]_2[\mathbf{4}]$, and $[NMe_3(CH_2Ph)][\mathbf{6}]$ are collected in Tables I–III, respectively. The ORTEP drawings of anions **3**, **4**, and **6** are shown in Figures 2–4, respectively. The molecular geometry of the three anions is based on octahedral

Table II. Selected Distances (Å) and Angles (deg) in the Dianion $[HFeIr_5(CO)_{15}]^{2-}$ (**4**) with Esd's on the Last Figure in Parentheses

Ir(1)–Ir(2)	2.771 (1)	Ir(2)–Fe(6)	2.669 (3)
Ir(1)–Ir(3)	2.696 (1)	Ir(3)–Ir(5)	2.823 (1)
Ir(1)–Ir(4)	2.796 (1)	Ir(3)–Ir(6)	2.757 (3)
Ir(1)–Ir(5)	2.868 (1)	Ir(4)–Ir(5)	2.696 (1)
Ir(2)–Ir(3)	2.780 (1)	Ir(4)–Fe(6)	2.821 (3)
Ir(2)–Ir(4)	2.768 (1)	Ir(5)–H	1.60 (9)
	Average Values[a]		
M–M	2.763	$M–C_t$	1.840 (18)[b]
$C–O_t$	1.156 (20)[b]	$M–C_b$	2.034 (16)[b]
$C–O_b$	1.712 (16)[b]		
$M–C_t–O_t$	177.2 (1.9)[b]	$M–C_b–O_b$	138.3 (1.4)[b]

[a] Key: M = metal; t = terminal; b = bridging. [b] The numbers in parentheses for the average values are the typical esd's of the single values before averaging.

Table III. Selected Distances (Å) and Angles (deg) in the Monoanion $[FeIr_5(CO)_{16}]^-$ (**6**) with Esd's on the Last Figure in Parentheses

Ir(1)–Ir(2)	2.784 (1)	Ir(7)–Ir(8)	2.764 (1)
Ir(1)–Ir(3)	2.770 (1)	Ir(7)–Ir(9)	2.742 (1)
Ir(1)–Ir(4)	2.769 (1)	Ir(7)–Ir(10)	2.782 (1)
Ir(1)–M(5)	2.750 (1)	Ir(7)–M(11)	2.756 (2)
Ir(2)–Ir(3)	2.729 (1)	Ir(8)–Ir(9)	2.758 (1)
Ir(2)–Ir(4)	2.786 (1)	Ir(8)–Ir(10)	2.802 (1)
Ir(2)–M(6)	2.780 (1)	Ir(8)–M(12)	2.743 (1)
Ir(3)–M(5)	2.819 (1)	Ir(9)–M(11)	2.768 (2)
Ir(3)–M(6)	2.819 (2)	Ir(9)–M(12)	2.815 (1)
Ir(4)–M(5)	2.770 (1)	Ir(10)–M(11)	2.733 (2)
Ir(4)–M(6)	2.725 (2)	Ir(10)–M(12)	2.747 (1)
M(5)–M(6)	2.794 (2)	M(11)–M(12)	2.840 (2)
	Average Values[a]		
M–M	2.773	$M–C_t$	1.821 (20)[b]
$C–O_t$	1.153 (20)[b]	$M–C_f$	2.195 (20)[b]
$C–O_f$	1.198 (20)[b]		
$M–C_t–O_t$	176.3 (1.8)[b]	$M–C_f–O_f$	132.9 (1.5)[b]

[a] Key: M = metal; t = terminal; f = face bridging. [b] The numbers in parentheses for the average values are the typical esd's of the single values before averaging.

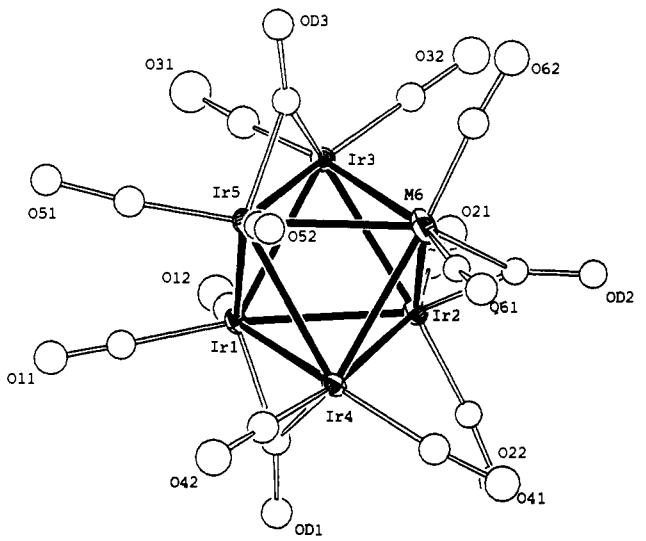

Figure 2. ORTEP drawing and atom-labeling scheme for $[FeIr_5(CO)_{15}]^{3-}$ (**3**). Thermal ellipsoids are drawn at 30% probability. Carbonyl carbons are designated in a manner analogous to the oxygens to which they are attached.

frameworks of metal atoms, with the characteristic 86 cluster valence electrons.

The positions of the metals and ligands are reasonably well-defined in all three compounds, and no misorientation of the metal frameworks is observed. Instead, for the vertices of the three octahedra, different degrees of substitutional disorder within the

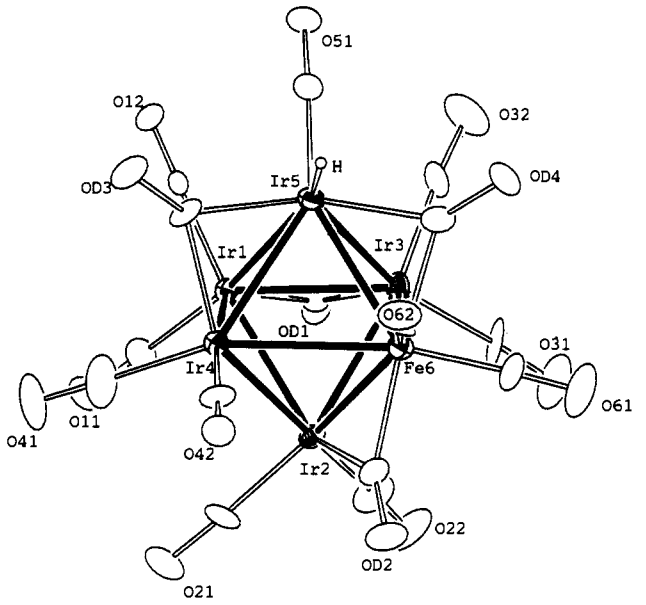

Figure 3. ORTEP drawing and atom-labeling scheme for $[HFeIr_5(CO)_{15}]^{2-}$ (**4**). Thermal ellipsoids are drawn at 30% probability. Carbonyl carbons are designated in a manner analogous to the oxygens to which they are attached.

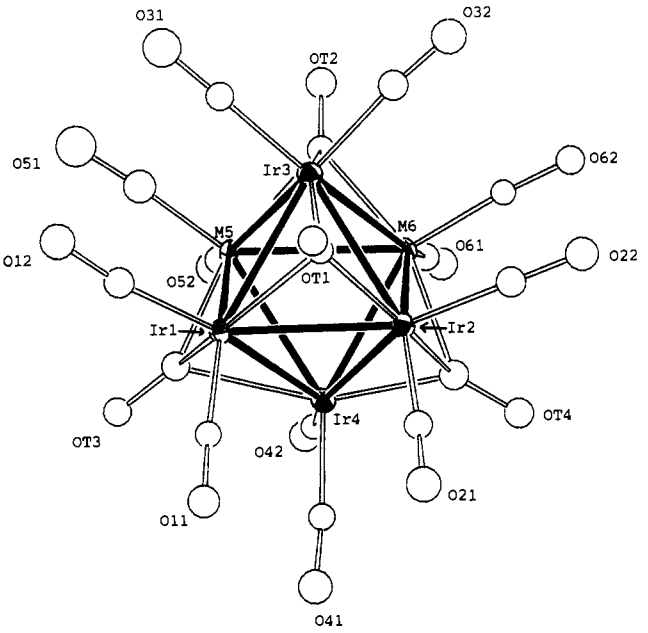

Figure 4. ORTEP drawing and atom-labeling scheme for $[FeIr_5(CO)_{16}]^-$ (**6**). Thermal ellipsoids are drawn at 30% probability. Carbonyl carbons are designated in a manner analogous to the oxygens to which they are attached.

metals were found (see Experimental Section): in anion **3**, despite the preferential location of iron in one of the vertices (labeled as M(6) and M(12) in the two independent moieties) of the octahedron, the remaining iron content is delocalized all over the other five positions; this disorder somehow affects the carbonyl ligand geometries, although they show satisfactory isotropic thermal parameters. Similarly, in anion **4**, the presence of a small fraction (14%) of Ir in the Fe(6) site was detected. In **6** only two cis positions of the octahedral framework are affected by disorder, with slightly different iron contents (60% and 40%).

In anion cluster **3** each metal is bonded to one edge bridging and two terminal carbonyls and each μ-CO connects different pairs of cluster vertices. This disposition is reminiscent of that found in $[Ir_6(CO)_{15}]^{2-}$,[7] of idealized D_3 symmetry, from which it can be formally derived by substituting an iridium atom with an isoelectronic Fe(-1) group.

The same formal and structural analogy holds for **6** and the red isomer of $Ir_6(CO)_{16}$,[8] with idealized T_d symmetry: thus, $[FeIr_5(CO)_{16}]^-$ possesses four face bridging ligands (on nonadjacent faces of the octahedron) and 12 terminal carbonyls: each metal is then connected to two terminal and two μ_3-CO groups. In the hydride derivative **4**, four edge bridging carbonyls are present: three connect different couples of metal atoms, the fourth spans the Ir(5)–Fe(6) edge; these two metal atoms are therefore bonded to two μ-CO ligands each. Ir(5) bears the terminal hydride (directly located from the X-ray data) and only one terminal carbonyl. The refined Ir–H distance is 1.60 (9) Å. $[HIr_4(CO)_{11}]^-$ is the only other hydridic iridium cluster structurally characterized, and the hydride was located by a neutron diffraction analysis in an edge-bridging position with Ir–H distances of 1.834 (13) Å.[9] The two values are in agreement, considering that terminal metal–H bond lengths are typically about 0.15 Å shorter than bridging distances[10] and that the two structures were determined with two different diffractometric methods. The homometallic hydrido cluster $[HIr_6(CO)_{15}]^-$ is known to exist,[11] but its structure is not available yet; **4** represents a reasonable model for its structure. Despite the low symmetry of **4** (C_1), its ligand arrangement must not be considered fortuitous: the hydrogen is bound to Ir, the heaviest element in the complex,[10] and tilts one of the terminal carbonyls in $[FeIr_5(CO)_{15}]^{3-}$ toward a μ-bridging mode, allowing the transfer of electron density from the electron richer Ir(5) to the more electron-deficient Fe(6) metallic site. Accordingly, atomic residual charge calculations predict Fe(6) to be more positive than Ir(5).[12]

The polyhedra described by the oxygen atoms of anions **3** and **6** are very symmetric (idealized symmetry D_3 and T_d, respectively), all metal vertices being topologically equivalent with respect to metal and ligand connectivity. Given that (i) the two nonhydridic species can exist in one isomer only and (ii) the positions of the oxygen atoms are slightly affected by the distribution of the metals in the metallic core, only weak packing forces and dipolar interactions between the ionic units of the lattice determine the site preferences for iron and iridium. Remarkably, the result of these weak *inter*molecular forces is such that, for both compounds, the independent units in the crystal lattice are very similar as far as the number of positions affected by disorder, their relative locations, and the occupation numbers are concerned. On the other hand, in **4** the presence of one hydride ligand produces a definite lowering of the idealized symmetry of the cluster. The substitutional disorder found at the metal sites can imply (i) the presence of different isomers, with a metal cage rotated within an unchanged ligand shell, or (ii) the presence of a single isomer, in different orientations. Presumably, intermolecular packing forces drive the hydrogen and the Ir(5) atoms in the same position in the unit cell: therefore, the disorder would also affect the remaining metal atoms and their attached bridging carbonyl groups, but not the terminal carbonyl ligands, which are identical at each metal site. However, no disorder of the ligands could be experimentally detected, because of its small extension.

In **6**, the two crystallographically independent molecules have similar structural parameters. The two independent moieties of compound **3**, however, show a variety of metal–metal bond distances and slightly different average bonding parameters, thus confirming that small metal clusters can easily be deformed in order to be accommodated in slightly different packing environments.[8] The average metal–metal bonds are 2.767 Å in **3**, 2.763 Å in **4**, and 2.773 Å in **6**. Owing to the significant substitutional disorder found in all three compounds, the metal–metal inter-

(8) Garlaschelli, L.; Martinengo, S.; Bellon, P. L.; Demartin, F.; Manassero, M.; Chiang, M. Y.; Wey, C. Y.; Bau, R. *J. Am. Chem. Soc.* **1984**, *106*, 6664.
(9) Bau, R.; Chiang, M. Y.; Wei, C. Y.; Garlaschelli, L.; Martinengo, S.; Koetzle, T. F. *Inorg. Chem.* **1984**, *23*, 4758.
(10) Teller, R. G.; Bau, R. *Struct. Bonding* **1981**, *44*, 1 and references therein.
(11) Della Pergola, R.; Garlaschelli, L.; Martinengo, S. To be submitted for publication.
(12) Ciani, G. Molecole. A local program for molecular drawings and molecular dynamics. Charge calculations performed according to: Sanderson, R. T. *J. Am. Chem. Soc.* **1983**, *105*, 2259.

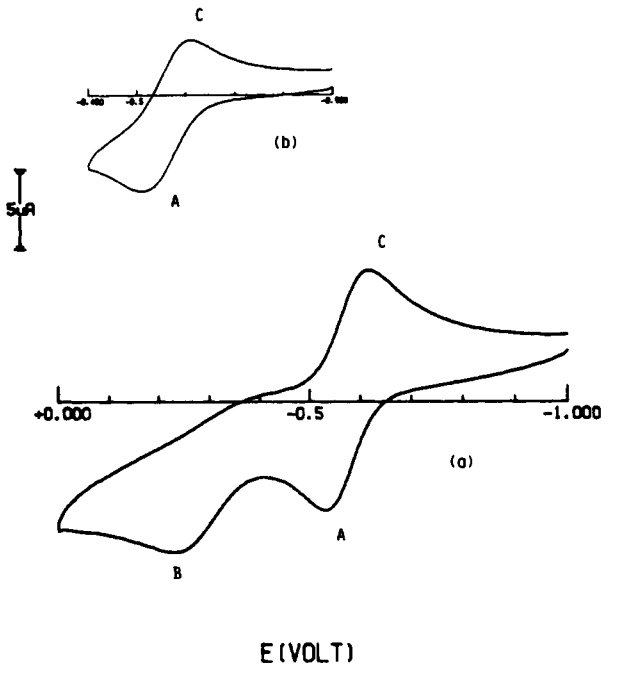

Figure 5. Cyclic voltammograms recorded at a platinum electrode on a deaerated MeCN solution containing $[FeIr_5(CO)_{15}]^{3-}$ (6.6×10^{-4} mol dm^{-3}) and $[NEt_4]ClO_4$ (0.2 mol dm^{-3}). Scan rate: (a) 0.2 V s^{-1}; (b) 0.5 V s^{-1}.

actions cannot be discussed in detail. They show typical values and do not seem affected either by the negative charges present in the different compounds or by the presence of different number and coordination modes of the bridging ligands. It must be noted, however, that the sites refined with a high iron content typically show shorter bond distances than those displayed by "pure" iridium ones. The lists of average metal–C and C–O bond distances for terminal, edge-bridging and face-bridging carbonyl ligands are consistent (i) with the local coordination geometries and the different π^* acidity of the different types of CO groups and, (ii) in compounds **3** and **6**, with the correlation between the net charge of the cluster and the consequent back-donation toward the ligands. The direct comparison of bond distances of **4** with those of **3** and **6** is however biased by the presence of the so-called "sliding effect"[13] of isotropically refined carbonyls and of the different thermal vibration models in complexes **3**, **4**, and **6**.

Electrochemistry Study. $[FeIr_5(CO)_{16}]^-/[FeIr_5(CO)_{15}]^{3-}$ Interconversion: The Redox Path. Figure 5 shows the cyclic voltammetric response exhibited by $[FeIr_5(CO)_{15}]^{3-}$ in acetonitrile solution. Two subsequent oxidation processes are displayed in correspondence with peaks A and B, respectively, with only the first one showing a directly associated response, peak C, in the reverse scan. Controlled-potential coulometry performed at the potential of the first step (E_w = −0.45 V) consumes 1 electron/molecule. Analysis[14] of the cyclic voltammograms of the peak-system A/C with scan rates varying from 0.02 to 20.48 V s^{-1} shows that (i) the peak current ratio $i_{p(C)}/i_{p(A)}$, which is equal to 0.8 at 0.02 V s^{-1}, reaches unity at 0.10 V s^{-1}, (ii) the current function $i_{p(A)}v^{-1/2}$ remains practically constant, and (iii) the peak-to-peak separation ($E_{p(A)} - E_{p(C)} = \Delta E_p$) progressively increases from 73 to 235 mV (under the same experimental conditions, the one-electron oxidation of ferrocene ($E^{\circ\prime}$ = +0.38 V) displays an increase in ΔE_p from 67 to 260 mV). These parameters are diagnostic for a substantially reversible one-electron-transfer step, complicated by slow, following chemical reactions. Assuming the occurrence of a first-order decomposition process, a half-life of about 20 s can be computed for the electrogenerable

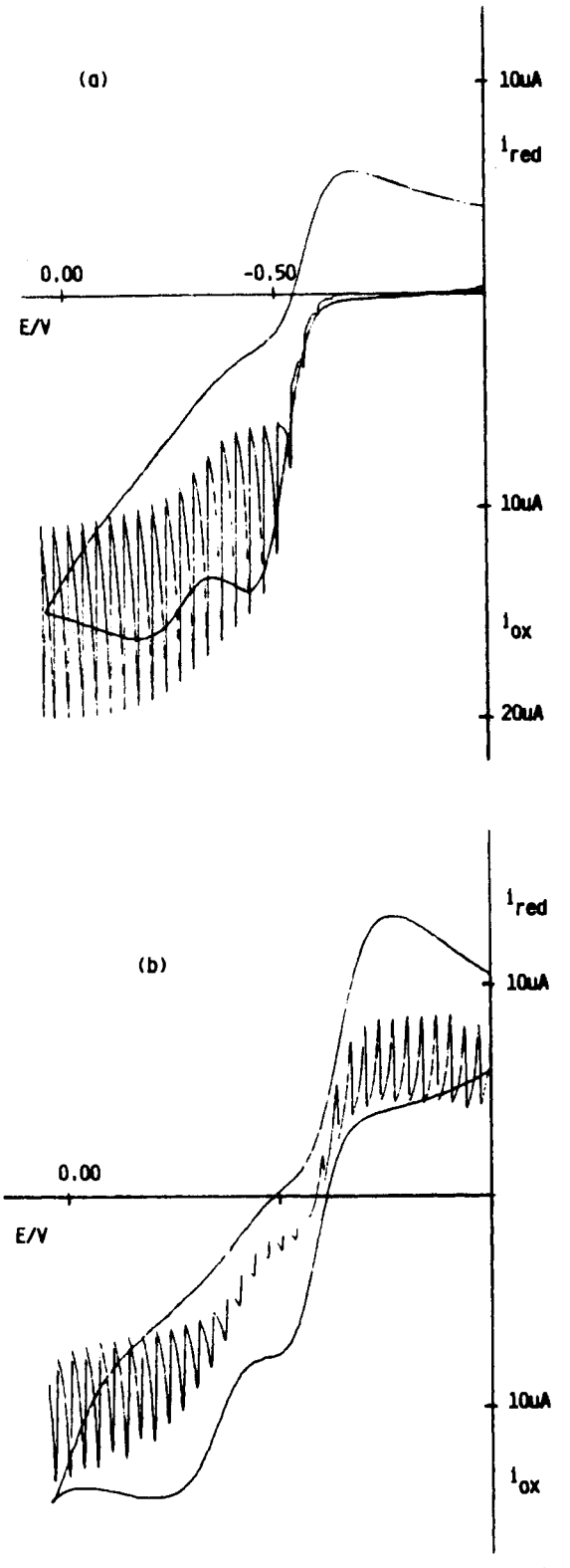

Figure 6. Cyclic and direct current voltammograms recorded at a platinum electrode on a deaerated MeCN solution containing $[N(PPh_3)_2]_3[FeIr_5(CO)_{15}]$ (1.83×10^{-3} mol dm^{-3}) and $[NEt_4]ClO_4$ (0.2 mol dm^{-3}): (a) initial scan; (b) scan after 0.7 electron/molecule was spent in controlled-potential electrolysis (E_w = −0.4 V). Temperature: −20 °C. Scan rate: CV, 0.2 V s^{-1}; DCV, 0.01 V s^{-1}. Potential values are given vs Ag/AgCl.

dianion $[FeIr_5(CO)_{15}]^{2-}$. Since, according to the Marcus theory,[15] the rate of an electron transfer (which is here directly related to the extent of electrochemical reversibility)[16-18] is an index of the

(13) Braga, D.; Koetzle, T. F. *J. Chem. Soc., Chem. Commun.* **1987**, 144. Albano, V. G.; Braga, D.; Grepioni, F. *Acta Crystallogr.* **1989**, *B45*, 60.

(14) Brown, E. R.; Sandifer, J. In *Physical Methods of Chemistry: Electrochemical Methods*; Rossiter, B. W., Hamilton, J. F., Eds.; Wiley: New York, 1986; Vol. 2, Chapter 4.

(15) Marcus, R. A.; Sutin, N. *Biochim. Biophys. Acta* **1985**, *265*, 811.

Table IV. Crystallographic Data for Compounds $[NEt_4]_3[FeIr_5(CO)_{15}]$ ($[NEt_4]_3$[3]), $[NMe_3(CH_2Ph)]_2[HFeIr_5(CO)_{15}]$ ($[NMe_3(CH_2Ph)]_2$[4], and $[NMe_3(CH_2Ph)][FeIr_6(CO)_{16}]$ ($[NMe_3(CH_2Ph)]$[6])[a]

compound	$[NEt_4]_3$[3]	$[NMe_3(CH_2Ph)]_2$[4]	$[NMe_3(CH_2Ph)]$[6]
chem formula	$C_{39}H_{60}FeIr_5N_3O_{15}$	$C_{35}H_{33}FeIr_5N_2O_{15}$	$C_{26}H_{16}FeIr_5NO_{16}$
fw	1827.77	1738.50	1615.26
a, Å	18.827 (5)	10.218 (3)	9.727 (2)
b, Å	19.476 (6)	10.989 (4)	16.296 (2)
c, Å	18.064 (5)	20.757 (5)	22.056 (2)
α, deg	117.06 (3)	101.07 (2)	79.99 (1)
β, deg	90.76 (2)	97.61 (2)	80.61 (2)
γ, deg	61.71 (2)	108.13 (2)	83.83 (1)
V, Å^3	5018 (4)	2127 (3)	3386 (1)
Z	4	2	4
d_{calc}, g/mL^3	2.419	2.714	3.169
μ(Mo Kα), cm^{-1}	135.04	159.22	199.96
min/max transm factor	0.46–1.00[b]	0.86–1.27[c]	0.31–1.00[b]
$R(F_o)$	0.040	0.041	0.041
$R_w(F_o)$	0.046	0.048	0.053

[a] Details common to all three compounds: crystal system, triclinic; space group, $P\bar{1}$; Mo Kα radiation, λ = 0.710 69 Å; temperature, 25 °C. [b] ψ scan corrections. [c] DIFABS corrections.

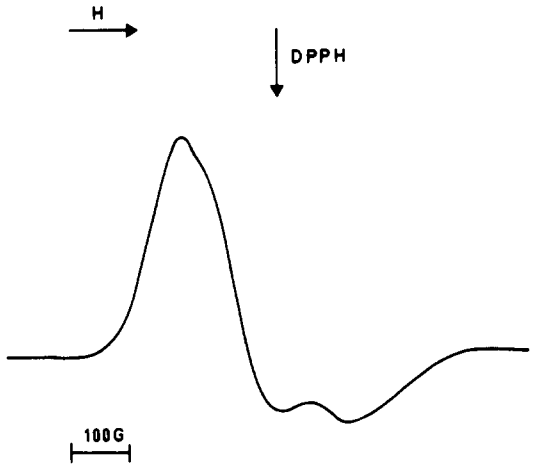

Figure 7. X-Band ESR spectrum, at 100 K, of the electrogenerated $[FeIr_5(CO)_{15}]^{2-}$ in MeCN solution.

Scheme I. Redox Behavior of $[FeIr_5(CO)_{15}]^{3-}$ (3)

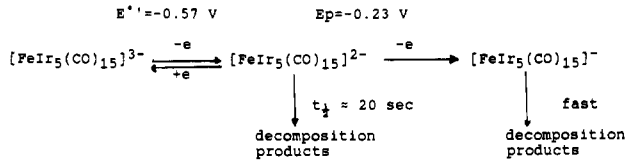

accompanying structural reorganizations, we foresee that the dianion substantially maintains the geometry of the starting trianion. The overall redox propensity of $[FeIr_5(CO)_{15}]^{3-}$ can be hence schematized as shown in Scheme I. We could not ascertain whether the relative instability of $[FeIr_5(CO)_{15}]^{2-}$ arises, as usual in carbonyl clusters,[17,18] from decarbonylation reactions, since, under CO atmosphere, the starting trianion tends to decompose.

The slowness of the dianion decomposition prompted us to investigate its paramagnetism. In order to further slow down the rate of the side reactions, controlled-potential electrolysis tests were performed at low temperature (−20 °C). As deducible from Figure 6, the electrogenerated dianion is rather stable in the longer times of electrolysis. Figure 7 shows the X-band ESR spectrum of the electrogenerated dianion, recorded at 100 K. The absorption line exhibits a well-resolved axial structure, with $g_\perp > g_\parallel$, typical for an unpaired electron ($S = {}^1/_2$). The relevant parameters are as follows: $g_\perp = 2.042 \pm 0.005$; $g_\parallel = 1.922 \pm 0.005$; g_{iso}(calc) $= {}^1/_3(g_\parallel + 2g_\perp) = 2.003 \pm 0.005$; $\Delta H_{\perp/\parallel} = 298 \pm 2$ G. The signal shows a remarkable dependence on temperature for both its intensity and its line shape. In fact, raising the temperature to the glass–liquid transition (ca. 140 K) causes a significant decrease of the spectral intensity accompanied by evolution toward a "pseudoorthorhombic" profile. Here, the anisotropic parameters become $g_l = 2.106 \pm 0.05$, $g_m = 2.017 \pm 0.005$, $g_h = 1.925 \pm 0.005$, and $\Delta H_{l/h} = 300 \pm 2$ G. Above the transition-phase temperature, the sample becomes ESR silent. It must be noted that, at the phase transition, a further, relatively intense extra signal suddenly arises ($\bar{g} = 2.01 \pm 0.01$; $\Delta H = 30 \pm 5$ G), partially

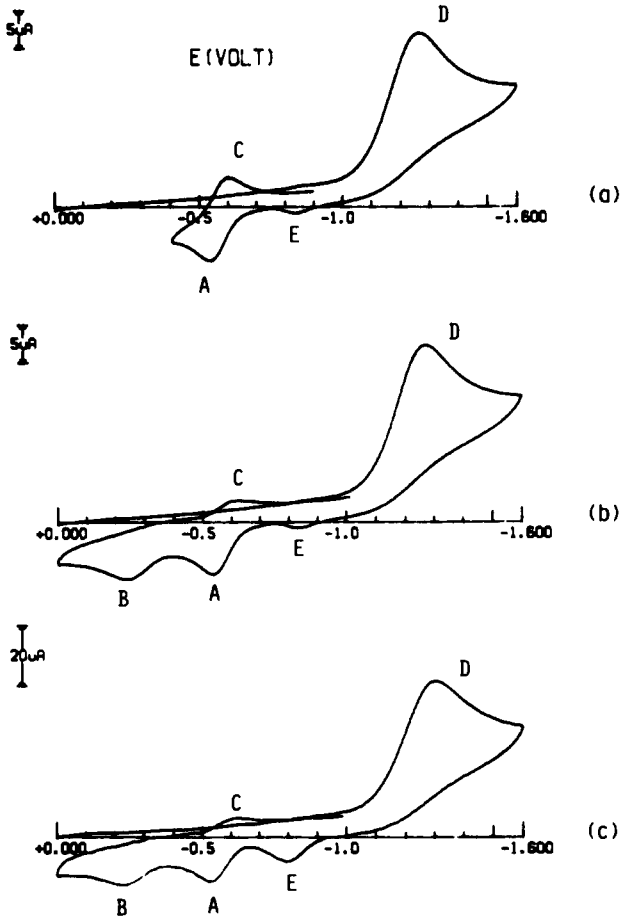

Figure 8. Cyclic voltammetric responses recorded at a platinum electrode on a deaerated MeCN solution containing $[N(PPh_3)_2][FeIr_5(CO)_{16}]$ (1.00×10^{-3} mol dm^{-3}) and $[NEt_4]ClO_4$ (0.2 mol dm^{-3}). Scan rate: (a, b) 0.2 V s^{-1}; (c) 1.0 V s^{-1}.

(16) Zanello, P. In *Stereochemistry of Organometallic and Inorganic Compounds*; Bernal, I., Ed.; Elsevier: Amsterdam, 1990, Vol. 4, Chapter 3.
(17) Zanello, P. In *Stereochemistry of Organometallic and Inorganic Compounds*; Bernal, I., Ed.; Elsevier: Amsterdam, 1991; Vol. 5.
(18) Zanello, P. *Structure and Bonding (Berlin)*; Springer Verlag: in press.

Scheme II. Redox Behavior of $[FeIr_5(CO)_{16}]^-$ (6)

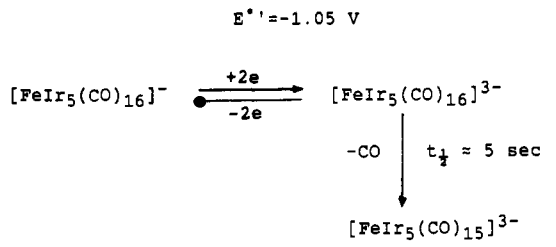

overlapping the previous one, likely attributable to metal–carbonyl fragments[19,20] arising from the relative instability of the dianion. The second-derivative spectrum at 100 K did not exhibit hyperfine splitting due to the interaction with the iridium nuclei ($I = {}^3/_2$), and no iridium satellite peaks were detected. The bulk of these data points out an unpaired electron, decidedly metal in character, that is delocalized over the entire cluster.

Figure 8 shows the redox fingerprint of $[FeIr_5(CO)_{16}]^-$ in acetonitrile solution. It undergoes a reduction process at peak D ($E_{p(0.2V_s^{-1})} = -1.27$ V), which by generation of the species able to be reoxidized through the peak-system profiles A/C and B (fully coincident with those reported in Figure 5) undoubtedly points out the electrogeneration of $[FeIr_5(CO)_{15}]^{3-}$. In confirmation of this evidence, controlled potential coulometry ($E_w = -1.5$ V) consumes two electrons/molecule, affording quantitatively the trianion $[FeIr_5(CO)_{15}]^{3-}$. A few comments have to be made about reoxidation peak E. In fact, such a peak, undetectable at scan rates lower than 0.2 V s^{-1}, increases at higher scan rates. The $i_{p(E)}/i_{p(D)}$ ratio, which is 0.02 at 0.2 V s^{-1}, progressively increases up to 0.25 at 10.24 V s^{-1}; at higher scan rates, peaks E and A tend to merge, making difficult the relative peak-height evaluation. The picture does not change by performing the measurements under CO atmosphere. We confidently attribute such anodic peak to the reoxidation of the transient $[FeIr_5(CO)_{16}]^{3-}$, which has been assigned a lifetime of about 5 s. The bulk of the data supports an interconversion pathways of the type shown in Scheme II.

It is useful to note that an electrochemically reversible two-electron step is theoretically characterized by a peak-to-peak separation constantly equal to 29 mV.[14] In actuality, the difference $E_{p(E)} - E_{p(D)}$ is 438 mV at 0.2 V s^{-1}, and it increases further with scan rate up to 630 mV at 10.24 V s^{-1}. This significant departure from electrochemical reversibility likely indicates that the addition of two electrons to $[FeIr_5(CO)_{16}]^-$ induces such a deep structural strain that it can only be relieved by CO release. This also suggests that the two electrons enter in antibonding orbitals, which are mainly centered on the peripheral carbonyl ligands.

Experimental Section

All the solvents were purified and dried by conventional methods and stored under nitrogen. All the reactions were carried out under oxygen-free nitrogen atmosphere by using the Schlenk-tube technique.[21] $Ir_4(CO)_{12}$,[22] $[N(PPh_3)_2][Ir(CO)_4]$,[6] $[Ir(CO)_2Cl_2]^-$,[23] and $[FeIr_4(CO)_{15}]^{2-}$[3] were prepared as already described. $Ir(CO)_3Br$ was purchased from Strem and used as received. Infrared spectra (IR) were recorded on a Perkin-Elmer 781 grating spectrophotometer using calcium fluoride cells previously purged with N_2. ^1H NMR spectra were recorded at 200 MHz on a Bruker AC200 spectrometer and are reported in ppm (parts per million) downfield from the internal standard $SiMe_4$. Samples for mass spectrometry were suspended in a matrix of *m*-nitrobenzyl alcohol/sulfolane and bombarded with a beam of xenon atoms at 70 keV with a VG Micromass machine; spectra were obtained by the staff of the Laboratorio Analisi, Università di Milano. Theoretical isotope patterns were calculated with the aid of the computer program ISO provided by the manufacturer. Calibration was checked before acquisition of data by using the reference spectrum of CsI clusters. Materials and apparatus for electrochemistry and ESR spectroscopy have been described elsewhere.[20] Direct current voltammograms at a platinum electrode with periodical renewal of the diffusion layer (DCV) have been obtained as

Table V. Fractional Atomic Coordinates for the Anion $[FeIr_5(CO)_{15}]^{3-}$ (3) with Esd's in Parentheses

atom	x	y	z
Ir(1)	0.23964 (6)	0.31141 (7)	0.41987 (7)
Ir(2)	0.33297 (6)	0.32588 (7)	0.31549 (7)
Ir(3)	0.36418 (6)	0.35178 (6)	0.47461 (7)
Ir(4)	0.35426 (6)	0.16198 (6)	0.27509 (7)
Ir(5)	0.39343 (6)	0.18708 (6)	0.43505 (7)
M(6)	0.4763 (3)	0.2006 (3)	0.3243 (4)
Ir(7)	0.74927 (6)	0.28172 (7)	0.87764 (7)
Ir(8)	0.85135 (7)	0.28090 (7)	0.98906 (7)
Ir(9)	0.88594 (6)	0.21609 (7)	0.74901 (7)
Ir(10)	0.82732 (6)	0.37605 (7)	0.90551 (7)
Ir(11)	0.90201 (6)	0.12436 (6)	0.83196 (7)
M(12)	0.9810 (2)	0.2206 (3)	0.8672 (3)
O(11)	0.151 (1)	0.262 (1)	0.500 (1)
O(12)	0.113 (1)	0.506 (1)	0.511 (1)
O(21)	0.272 (1)	0.523 (1)	0.400 (1)
O(22)	0.275 (1)	0.314 (1)	0.157 (1)
O(31)	0.241 (1)	0.495 (2)	0.646 (2)
O(32)	0.448 (1)	0.448 (1)	0.472 (1)
O(41)	0.432 (1)	0.087 (1)	0.091 (1)
O(42)	0.359 (1)	−0.000 (1)	0.259 (1)
O(51)	0.313 (1)	0.191 (1)	0.583 (1)
O(52)	0.533 (1)	−0.005 (1)	0.354 (1)
O(61)	0.593 (1)	0.012 (1)	0.197 (1)
O(62)	0.608 (1)	0.230 (1)	0.377 (1)
O(71)	0.657 (1)	0.252 (1)	0.745 (1)
O(72)	0.656 (1)	0.273 (1)	1.002 (1)
O(81)	0.763 (1)	0.454 (2)	1.156 (2)
O(82)	0.854 (1)	0.162 (1)	1.055 (1)
O(91)	0.792 (1)	0.256 (1)	0.623 (1)
O(92)	1.031 (1)	0.217 (1)	0.683 (1)
O(101)	0.818 (1)	0.445 (1)	0.782 (1)
O(102)	0.851 (1)	0.511 (1)	1.048 (1)
O(111)	1.042 (1)	−0.012 (1)	0.864 (1)
O(112)	0.789 (1)	0.052 (1)	0.819 (1)
O(121)	1.138 (1)	0.053 (1)	0.782 (1)
O(122)	1.046 (1)	0.335 (1)	0.887 (1)
O(D1)	0.177 (1)	0.253 (1)	0.261 (1)
O(D2)	0.5003 (9)	0.254 (1)	0.206 (1)
O(D3)	0.491 (1)	0.253 (1)	0.549 (1)
O(D4)	0.643 (1)	0.485 (1)	0.966 (1)
O(D5)	1.014 (1)	0.247 (1)	1.033 (1)
O(D6)	0.9587 (9)	0.016 (1)	0.640 (1)
C(11)	0.186 (2)	0.277 (2)	0.468 (2)
C(12)	0.166 (2)	0.425 (2)	0.468 (2)
C(21)	0.293 (2)	0.444 (2)	0.370 (2)
C(22)	0.298 (1)	0.322 (2)	0.218 (2)
C(31)	0.289 (2)	0.436 (2)	0.574 (2)
C(32)	0.409 (2)	0.416 (2)	0.476 (2)
C(41)	0.401 (2)	0.112 (2)	0.160 (2)
C(42)	0.357 (2)	0.066 (2)	0.266 (2)
C(51)	0.343 (2)	0.190 (2)	0.519 (2)
C(52)	0.479 (1)	0.068 (2)	0.386 (2)
C(61)	0.543 (1)	0.086 (2)	0.246 (2)
C(62)	0.554 (2)	0.219 (2)	0.360 (2)
C(71)	0.693 (2)	0.261 (2)	0.795 (2)
C(72)	0.693 (1)	0.277 (2)	0.956 (2)
C(81)	0.793 (2)	0.388 (2)	1.094 (2)
C(82)	0.851 (2)	0.209 (2)	1.027 (2)
C(91)	0.828 (2)	0.235 (2)	0.669 (2)
C(92)	0.977 (2)	0.217 (2)	0.718 (2)
C(101)	0.829 (2)	0.416 (2)	0.828 (2)
C(102)	0.841 (2)	0.460 (2)	0.992 (2)
C(111)	0.986 (1)	0.040 (2)	0.850 (2)
C(112)	0.836 (1)	0.081 (2)	0.825 (2)
C(121)	1.070 (2)	0.123 (2)	0.817 (2)
C(122)	1.014 (2)	0.295 (2)	0.877 (2)
C(D1)	0.228 (2)	0.247 (2)	0.304 (2)
C(D2)	0.461 (1)	0.254 (2)	0.257 (2)
C(D3)	0.442 (1)	0.261 (2)	0.503 (2)
C(D4)	0.707 (1)	0.413 (2)	0.933 (2)
C(D5)	0.971 (1)	0.247 (2)	0.984 (2)
C(D6)	0.932 (1)	0.087 (2)	0.706 (2)

(19) Osella, D.; Arman, G.; Botta, M.; Gobetto, R.; Laschi, F.; Zanello, P. *Organometallics* **1989**, *8*, 620.
(20) Osella, D.; Gambino, O.; Gobetto, R.; Zanello, P.; Laschi, F.; Housecroft, C. E.; Owen, S. M. *Organometallics* **1990**, *9*, 1792.
(21) Shriver, D. F.; Drezdzon, M. A. *The Manipulation of Air-Sensitive Compounds*, 2nd ed.; Wiley: New York, 1986.
(22) Della Pergola, R.; Garlaschelli, L.; Martinengo, S. *J. Organomet. Chem.* **1987**, *331*, 271.
(23) Forster, D. *Inorg. Nucl. Chem. Lett.* **1969**, *5*, 433.

Table VI. Fractional Atomic Coordinates for the Anion $[HFeIr_5(CO)_{15}]^{2-}$ (**4**) with Esd's in Parentheses

atom	x	y	z
Ir(1)	−0.02662 (7)	0.10524 (6)	0.29047 (3)
Ir(2)	−0.08270 (7)	0.16650 (7)	0.16871 (3)
Ir(3)	−0.20295 (7)	0.24093 (7)	0.27537 (4)
Ir(4)	0.18274 (7)	0.28965 (7)	0.25003 (3)
Ir(5)	0.07208 (8)	0.38370 (7)	0.35106 (3)
Fe(6)	−0.0091 (3)	0.4224 (3)	0.2291 (1)
O(11)	0.012 (2)	−0.144 (1)	0.2242 (8)
O(12)	0.055 (1)	0.093 (1)	0.4344 (5)
O(21)	0.049 (2)	−0.001 (2)	0.0855 (8)
O(22)	−0.376 (2)	0.022 (1)	0.0841 (7)
O(31)	−0.446 (2)	0.258 (2)	0.1862 (9)
O(32)	−0.307 (2)	0.310 (2)	0.4045 (9)
O(41)	0.310 (2)	0.073 (2)	0.223 (1)
O(42)	0.377 (1)	0.473 (1)	0.1847 (6)
O(51)	0.031 (2)	0.377 (1)	0.4919 (6)
O(61)	−0.204 (2)	0.534 (2)	0.1784 (9)
O(62)	0.231 (1)	0.668 (1)	0.2529 (6)
O(D1)	−0.338 (1)	−0.049 (1)	0.2704 (7)
O(D2)	0.007 (2)	0.364 (1)	0.0874 (6)
O(D3)	0.368 (1)	0.368 (1)	0.3871 (6)
O(D4)	−0.081 (2)	0.578 (1)	0.3463 (7)
C(11)	0.002 (2)	−0.041 (2)	0.250 (1)
C(12)	0.025 (1)	0.097 (1)	0.3795 (8)
C(21)	−0.001 (2)	0.066 (2)	0.1160 (9)
C(22)	−0.266 (2)	0.078 (2)	0.1167 (9)
C(31)	−0.353 (2)	0.252 (2)	0.222 (1)
C(32)	−0.261 (2)	0.283 (2)	0.356 (1)
C(41)	0.262 (2)	0.153 (2)	0.232 (1)
C(42)	0.303 (2)	0.403 (2)	0.2097 (8)
C(51)	0.051 (2)	0.387 (2)	0.438 (1)
C(61)	−0.132 (2)	0.489 (2)	0.199 (1)
C(62)	0.135 (2)	0.569 (2)	0.2438 (8)
C(D1)	−0.240 (2)	0.049 (2)	0.2736 (8)
C(D2)	−0.013 (2)	0.338 (2)	0.1370 (9)
C(D3)	0.265 (2)	0.353 (2)	0.3519 (8)
C(D4)	−0.038 (2)	0.494 (2)	0.3225 (9)
H	0.19 (1)	0.53 (1)	0.375 (5)

previously described.[24] Unless otherwise specified, potential values are referred to an aqueous saturated calomel electrode (SCE).

Preparation of $[PPh_4]_2[HFe_3Ir(CO)_{12}]$ ($[PPh_4]_2[1]$). $[PPh_4][Ir(CO)_2Cl_2]$ (0.318 g, 0.48 mmol) and $[NEt_4][HFe(CO)_4]$ (0.377 g, 1.27 mmol) are dissolved in acetone (25 mL) and refluxed for 8 h. The solution is then cooled and the solvent removed in a vacuum. The brown residue is suspended overnight in MeOH (20 mL) and collected by filtration. The microcrystalline product is washed with MeOH (2 × 5 mL), dried, extracted with acetone (8 mL), and layered with 2-propanol. Yield: 0.395 g, 60%. Anal. Calcd for $C_{60}H_{41}Fe_3IrO_{12}P_2$: C, 52.38; H, 2.98. Found: C, 49.4; H, 2.49. Elemental analyses are frequently unsatisfactory, probably because of cocrystallized impurities.

Preparation of $[NEt_4]_2[HFe_3Ir(CO)_{12}]$ ($[NEt_4]_2[1]$). In a round-bottomed flask are placed $[NEt_4][HFe(CO)_4]$, (0.30 g, 1.1 mmol), $Ir(CO)_3Br$ (0.13 g, 0.36 mmol), and thf (15 mL). The mixture is refluxed, with stirring, for 8 h. The solvent is removed in a vacuum and the crude brown residue suspended in 25 mL of MeOH. The microcrystalline powder is collected by filtration, washed with 2-propanol, and dried. It can be crystallized from acetone/2-propanol. Yield: 0.11 g, 33%. Anal. Calcd for $C_{28}H_{41}Fe_3IrN_2O_{12}$: C, 35.12; H, 4.28; N, 2.92. Found: C, 34.9; H, 4.43; N, 2.91.

Preparation of $[NEt_4][H_2Fe_3Ir(CO)_{12}]$ ($[NEt_4][2]$). The salt $[NEt_4]_2[HFe_3Ir(CO)_{12}]$ is dissolved in acetone, and 85% H_3PO_4 is added dropwise, while the solution is monitored by IR. When the starting material has reacted completely, the solvent is evaporated in a vacuum, and the reddish residue is dissolved in MeOH. The crude $[NEt_4][H_2Fe_3Ir(CO)_{12}]$ is precipitated by the addition of $[NEt_4]Cl$ and water. It is collected by filtration, washed with water, and crystallized from thf/cyclohexane.

Preparation of $[N(PPh_3)_2]_3[FeIr_5(CO)_{15}]$ ($[N(PPh_3)_2]_3[3]$). From $Ir_4(CO)_{12}$ (0.810 g, 0.72 mmol) and $Fe(CO)_5$ (0.1 mL) the compound $[N(PPh_3)_2]_2[FeIr_4(CO)_{15}]$ is prepared, as already described. The pentanuclear cluster is extracted from the frit with CH_3CN (30 mL), and solid $[N(PPh_3)_2][Ir(CO)_4]$ is added (0.555 g, 0.66 mmol). The solution is refluxed for 5 h. The solvent is evaporated in a vacuum, the oily residue is suspended in MeOH (30 mL), and the semisolid material is

(24) Zanello, P.; Bartocci, C.; Maldotti, A.; Traverso, O. *Polyhedron* **1983**, *2*, 791.

Table VII. Fractional Atomic Coordinates for the Anion $[FeIr_5(CO)_{16}]^-$ (**6**) with Esd's in Parentheses

atom	x	y	z
Ir(1)	1.01790 (8)	0.54123 (5)	0.61155 (4)
Ir(2)	0.89534 (8)	0.57067 (5)	0.72980 (4)
Ir(3)	1.16926 (9)	0.59870 (5)	0.68940 (4)
Ir(4)	0.94646 (9)	0.40795 (5)	0.70378 (4)
M(5)	1.2246 (1)	0.43492 (8)	0.66145 (6)
M(6)	1.0996 (2)	0.4599 (1)	0.78089 (8)
Ir(7)	0.52091 (8)	0.00487 (5)	0.19936 (4)
Ir(8)	0.32194 (8)	−0.10988 (5)	0.23594 (4)
Ir(9)	0.27877 (9)	0.04370 (5)	0.27538 (4)
Ir(10)	0.36495 (8)	−0.02810 (5)	0.11250 (4)
M(11)	0.3236 (2)	0.1231 (1)	0.1531 (1)
M(12)	0.1208 (1)	0.00408 (8)	0.18983 (6)
O(11)	0.748 (2)	0.561 (1)	0.5619 (8)
O(12)	1.189 (2)	0.628 (1)	0.4962 (9)
O(21)	0.606 (2)	0.612 (1)	0.6995 (9)
O(22)	0.840 (2)	0.649 (1)	0.8440 (8)
O(31)	1.403 (2)	0.668 (1)	0.595 (1)
O(32)	1.228 (2)	0.694 (1)	0.7858 (9)
O(41)	0.672 (2)	0.384 (1)	0.6666 (8)
O(42)	1.034 (2)	0.226 (1)	0.7321 (8)
O(51)	1.461 (2)	0.473 (1)	0.565 (1)
O(52)	1.346 (2)	0.262 (1)	0.6919 (9)
O(61)	1.181 (2)	0.295 (1)	0.8494 (8)
O(62)	1.081 (2)	0.5383 (9)	0.8910 (7)
O(71)	0.697 (2)	0.128 (1)	0.2294 (9)
O(72)	0.769 (2)	−0.109 (1)	0.1602 (8)
O(81)	0.483 (2)	−0.269 (1)	0.2028 (8)
O(82)	0.164 (2)	−0.191 (1)	0.3538 (8)
O(91)	0.057 (2)	0.001 (1)	0.3834 (9)
O(92)	0.388 (2)	0.174 (1)	0.332 (1)
O(101)	0.554 (2)	−0.167 (1)	0.0639 (8)
O(102)	0.225 (2)	0.023 (1)	−0.0015 (8)
O(111)	0.187 (2)	0.214 (1)	0.0476 (8)
O(112)	0.446 (2)	0.264 (1)	0.1769 (9)
O(121)	−0.058 (2)	0.071 (1)	0.0923 (8)
O(122)	−0.127 (1)	−0.0402 (8)	0.2831 (7)
O(T1)	0.952 (1)	0.7363 (9)	0.6399 (7)
O(T2)	1.413 (2)	0.475 (1)	0.7509 (8)
O(T3)	1.081 (1)	0.3735 (9)	0.5661 (7)
O(T4)	0.799 (2)	0.4151 (9)	0.8367 (7)
O(T5)	0.506 (1)	−0.0840 (9)	0.3359 (7)
O(T6)	0.046 (2)	0.1832 (9)	0.2304 (7)
O(T7)	0.583 (2)	0.1041 (9)	0.0599 (7)
O(T8)	0.129 (2)	−0.161 (1)	0.1500 (8)
C(11)	0.854 (2)	0.554 (1)	0.580 (1)
C(12)	1.116 (2)	0.592 (1)	0.539 (1)
C(21)	0.714 (2)	0.593 (1)	0.713 (1)
C(22)	0.859 (2)	0.622 (1)	0.798 (1)
C(31)	1.312 (2)	0.642 (1)	0.632 (1)
C(32)	1.212 (2)	0.660 (1)	0.748 (1)
C(41)	0.772 (2)	0.393 (1)	0.683 (1)
C(42)	0.994 (2)	0.293 (1)	0.722 (1)
C(51)	1.367 (3)	0.459 (2)	0.605 (1)
C(52)	1.300 (2)	0.332 (1)	0.680 (1)
C(61)	1.152 (2)	0.360 (1)	0.821 (1)
C(62)	1.094 (2)	0.508 (1)	0.846 (1)
C(71)	0.632 (2)	0.080 (1)	0.217 (1)
C(72)	0.674 (2)	−0.066 (1)	0.174 (1)
C(81)	0.422 (2)	−0.210 (1)	0.217 (1)
C(82)	0.228 (2)	−0.162 (1)	0.306 (1)
C(91)	0.141 (2)	0.017 (1)	0.343 (1)
C(92)	0.345 (2)	0.129 (1)	0.307 (1)
C(101)	0.483 (2)	−0.110 (1)	0.082 (1)
C(102)	0.282 (2)	−0.001 (1)	0.041 (1)
C(111)	0.242 (2)	0.180 (1)	0.090 (1)
C(112)	0.395 (2)	0.206 (1)	0.169 (1)
C(121)	0.009 (2)	0.046 (1)	0.131 (1)
C(122)	−0.032 (2)	−0.025 (1)	0.248 (1)
C(T1)	0.986 (2)	0.669 (1)	0.661 (1)
C(T2)	1.301 (2)	0.477 (1)	0.736 (1)
C(T3)	1.084 (2)	0.419 (1)	0.605 (1)
C(T4)	0.882 (2)	0.440 (1)	0.792 (1)
C(T5)	0.454 (2)	−0.057 (1)	0.290 (1)
C(T6)	0.133 (2)	0.128 (1)	0.216 (1)
C(T7)	0.496 (2)	0.075 (1)	0.100 (1)
C(T8)	0.184 (2)	−0.106 (1)	0.165 (1)

transformed into a microcrystalline precipitate. The pale yellow solution is decanted by syringe, and the solid is extracted twice with thf (15 mL), eliminating the soluble material (mainly $[N(PPh_3)]_2[HFeIr_5(CO)_{15}]$, 0.28 g). The residue is composed of $[N(PPh_3)_2]_3[FeIr_5(CO)_{15}]$ of good purity, which can be used without further purification. Yield: 1.4 g (62 %).

Other tetraalkylammonium salts were obtained through a double metathesis reaction. The $[N(PPh_3)_2]_3[FeIr_5(CO)_{15}]$ salt is suspended in acetone and the solution is treated with the stoichiometric amount of $Na[BPh_4]$, which causes the precipitation of the insoluble $[N(PPh_3)_2]$-BPh_4 and leaves in solution the sodium salt of the cluster. The insoluble salt is filtered off, the solvent is dried in vacuum, and the residue is dissolved with MeOH (20 mL) and treated with an excess of tetraalkylammonium halide, such as $[NEt_4]Cl$ or $[NMe_3(CH_2Ph)]Cl$, precipitating the corresponding salt in about 80% yield.

Crystals of $[NEt_4]_3[FeIr_5(CO)_{15}]$ suitable for X-ray analysis were obtained from the slow diffusion technique from CH_3CN/diisopropyl ether. Anal. Calcd for $C_{39}H_{60}FeIr_5N_3O_{15}$: C, 25.63; H, 3.29; N, 2.30. Found: C, 24.85; H, 3.18; N, 2.27.

Preparation of $[N(PPh_3)_2]_2[HFeIr_5(CO)_{15}]$ ($[N(PPh_3)_2]_2$[4]). $[N(PPh_3)_2]_3[FeIr_5(CO)_{15}]$ (0.45 g, 0.15 mmol) was suspended in acetone (10 mL) and treated dropwise with 85% H_3PO_4. After the addition of 0.3 mL, the mixture is allowed to react for 10 min, and the complete conversion of $[FeIr_5(CO)_{15}]^{3-}$ into $[HFeIr_5(CO)_{15}]^{2-}$ is checked by IR spectroscopy. The solvent is then evaporated in a vacuum and the residue is suspended in 2-propanol (10 mL) while being stirred. The brown compound is collected by filtration, and the crude product is dissolved in thf and crystallized with slow diffusion of 2-propanol. Yield: 0.3 g, 75%. The crystals obtained with this method contain clathrated thf and are not suitable for X-ray analysis. Anal. Calcd for $C_{91}H_{69}FeIr_5N_2O_{16}P_4$: C, 42.24; H, 2.67; N, 1.08. Found: C, 42.35; H, 2.44; N, 0.84.

Crystals of $[NMe_3(CH_2Ph)]_2[HFeIr_5(CO)_{15}]$ used for X-ray analysis were obtained by the same procedure, starting from $[NMe_3(CH_2Ph)]_3$-$[FeIr_5(CO)_{15}]$.

Preparation of $[N(PPh_3)_2]FeIr_5(CO)_{16}]$ ($[N(PPh_3)_2]$[6]). $[N(PPh_3)_2]_3[FeIr_5(CO)_{15}]$ (0.9 g, 0.3 mmol) is suspended in thf (15 mL). A 0.2-mL aliquot of concentrated sulfuric acid is slowly added, and the complete conversion is checked by IR spectroscopy. The mixture is stirred at room temperature for 2 h, and then the solvent is removed in a vacuum. The brown residue is dissolved in MeOH (30 mL), to remove excess acid and $[N(PPh_3)_2]_2SO_4$. The brown powder is collected by filtration, washed with 2-propanol and crystallized from CH_2Cl_2/cyclohexane. Yield: 0.36 g, 61%. Calcd for $C_{52}H_{30}FeIr_5NO_{16}P_2$: C, 31.17; H, 1.50; N, 0.70. Found: C, 30.9; H, 1.3; N, 0.50.

Crystals of $[NMe_3(CH_2Ph)][FeIr_5(CO)_{16}]$ used for X-ray analysis were obtained in the same way starting from $[NMe_3(CH_2Ph)]_3[FeIr_5$-$(CO)_{15}]$.

X-ray Crystal Structure Determinations of the Salts of 3, 4, and 6. Crystal data and experimental conditions for the salts of compounds **3**, **4**, and **6** are reported in Table IV. The intensity data were collected with an Enraf-Nonius CAD4 automated diffractometer and graphite-monochromatized Mo Kα radiation (λ = 0.71069 Å). A least-squares fit of 25 randomly reflections with θ ranging from 8 to 12° provided the unit-cell parameters. Three standard reflections were measured at regular intervals during data collection; decays of about 37% and 7% on Fobs for compounds **3** and **6**, respectively, were observed; the corresponding data sets were therefore corrected with a linear decay model. Intensities were collected by using a variable scan range with 25% extension at each end for background determination. Corrections for Lorentz and polarization effects were applied. Empirical absorption corrections were performed on the basis of ψ scans (0–360° every 10°) of three suitable reflections with χ values close to 90°. In addition, for compound **4**, a further absorption correction (DIFABS)[25] was applied to its full data set, after complete isotropic refinement; this was suggested by the presence of ghost peaks around the metal atoms and some poorly defined thermal ellipsoids of the lighter atoms at the end of complete refinement on the data set corrected with ψ scans only.

The structure of compound **4** was solved with standard Patterson and Fourier methods, while the heavy atoms of compounds **3** and **6** were located by direct methods (MULTAN).[26] Full matrix least-squares refinements were performed using the Enraf-Nonius Structure Determination Package (SDP)[27] and the physical constants tabulated therein on a PDP 11/73 computer. Atomic scattering factors, corrected for real and imaginary anomalous dispersion terms, were taken from ref 28.

The final values of the agreement indices are reported in Table IV. A certain degree of substitutional disorder was observed in all three compounds between the Fe sites and some Ir sites. Several refinements of the occupancy factors of these two atoms were performed, keeping unitary the occupancy fractions for all the atoms of the ligands and of the cations. The refined values were than used for computing mixed-atom scattering factors, which were subsequently introduced in the final least-squares refinement cycles as follows: 80% Fe + 20% Ir for site M(6) and 75% Fe + 25% Ir for site M(12) in **3**; 86% Fe + 14% Ir for the site labeled as Fe(6) in **4**; 60% Fe + 40% Ir for sites M(6) and M(11) and 40% Fe + 60% Ir for sites M(5) and M(12) in **6**; for all other metallic sites, where the iridium percentage is higher than 96%, the small iron fractions (if any) have been simulated by using occupancy numbers for iridium atoms slightly smaller than 1.00 [Ir(1) to Ir(5) = 0.97 and Ir(7) to Ir(11) = 0.96 for **3**; Ir(1) to Ir(4) = 0.98 and Ir(5) = 1.00 for **4**; Ir(1) to Ir(4) and Ir(7) to Ir(10) = 1.00 for **6**].

Anisotropic thermal parameters were assigned to all metal atoms of the three compounds and to the carbonyl atoms of $[NMe_3(CH_2Ph)]_2$[4], while isotropic thermal parameters were assigned to all the remaining atoms. The hydrogen atom in the anion of $[NMe_3(CH_2Ph]_2$[4] was directly localized from a Fourier map and refined. Hydrogen atoms of the cations of $[NMe_3(CH_2Ph)]_2$[4] and $[NMe_3(CH_2Ph)]$[6] were fixed in their ideal positions (C–H = 0.95 Å) after each cycle of refinement (B = 7.0 Å^2) but not refined. The contribution of the hydrogen atoms of $[NEt_4]_3$[3] was omitted in the structure factor calculation because some of the cations show carbon atoms with high thermal parameters and poor bonding geometries, suggesting the presence of some kind of conformational disorder of the aliphatic chains. The highest peaks in the final difference Fourier maps of the three compounds were 1.7, 2.3, and 2.1 e/Å^3, respectively, mostly located in proximity to the metallic frameworks. The final values of the positional parameters of anions **3**, **4**, and **6** are reported in Tables V–VII, respectively.

Registry No. $[PPh_4]_2$[1], 134681-79-1; $[NEt_4]_2$[1], 134681-80-4; $[N(PPh_3)_2]_3$[3], 134681-82-6; $[NEt_4]_3$[3], 134681-83-7; $[NMe_3(CH_2Ph)]_3$[3], 134681-86-0; [3]$^{2-}$, 134681-91-7; $[N(PPh_3)_2]_2$[4], 134681-85-9; $[NMe_3(CH_2Ph)]_2$[4], 134733-22-5; $[N(PPh_3)_2]$[6], 134681-88-2; $[NMe_3(CH_2Ph)]$[6], 134681-90-6; $[PPh_4][Ir(CO)_2Cl_2]$, 121872-75-1; $[NEt_4][HFe(CO)_4]$, 25879-01-0; $Ir(CO)_3Br$, 17836-58-7; $Ir_4(CO)_{12}$, 18827-81-1; $Fe(CO)_5$, 13463-40-6; $[N(PPh_3)_2][Ir(CO)_4]$, 56557-01-8; Ir, 7439-88-5; Fe, 7439-89-6.

Supplementary Material Available: Tables of anisotropic and isotropic thermal parameters, fractional atomic coordinates for cation atoms, complete bond distances and angles, calculated positional parameters for cation hydrogens, and complete crystallographic data (44 pages); tables of observed and calculated structure factors (105 pages). Ordering information is given on any current masthead page.

(25) Walker, N.; Stuart, D. *Acta Crystallogr.* **1983**, *A39*, 158.

(26) Germain, G.; Main, P.; Woolfson, M. M. MULTAN, a system of computer programs for the automatic solution of crystal structures from X-ray diffraction data. *Acta Crystallogr.* **1971**, *A27*, 368.

(27) Frenz, B. A. and Associates. *SDP Plus Version 1.0*, Enraf-Nonius: Delft, The Netherlands, 1980.

(28) *International Tables for X-Ray Crystallography*; Kynoch Press: Birmingham, England, 1974; Vol. 4.